Somatic mutations reveal clonal cell populations in atherosclerotic plaques

Steffensen LB[1,2], Dembic M[3,4,5], Jensen PS[2,6], Andersen LvB[3], Lindholt JS[2,7], Houlind KC[8], Thomassen M[3], *Rasmussen LM[2,6]

1. Dept. of Molecular Medicine, University of Southern Denmark, Odense, Denmark
2. Centre for Individualized Medicine in Arterial Diseases (CIMA), Odense University Hospital, Odense, Denmark
3. Dept. of Clinical Genetics, Odense University Hospital, Odense, Denmark
4. Dept. of Mathematics and Computer Science (IMADA), University of Southern Denmark, Odense, Denmark
5. Dept. of Clinical Research, University of Southern Denmark, Odense, Denmark
6. Dept. of Clinical Biochemistry and Pharmacology, Odense University Hospital, Odense, Denmark
7. Dept. of Cardiothoracic Surgery, Odense University Hospital, Odense, Denmark
8. Dept. of Regional Health Research, Lillebælt Hospital, Kolding, Denmark

***Corresponding author:**

Lars Melholt Rasmussen

J. B. Winsløws Vej 4, 5000 Odense C, Denmark

Phone: 0045-65414506

Mail: lars.melholt.rasmussen@rsyd.dk

Word count (excl. abstract, figure legends and references): 3372

Figures: 2

Supplementary figures: 6

Supplementary tables: 4

ABSTRACT

In recent years, the potential involvement of clonal cell populations in atherosclerosis has emerged. Evidence from independent research groups unambiguously showed that smooth muscle cells clonally expand in experimental atherosclerosis, and clonal hematopoiesis of indeterminate potential (CHIP) was identified as a novel independent risk factor for atherosclerotic cardiovascular disease. However, whether clonal cell populations contribute to human atherosclerotic lesions remains elusive.

In this study, we performed deep whole-exome sequencing of 32 segments from 14 carotid plaques of patients undergoing carotid endatherectomy. We unveiled a landscape of somatic mutations confined to plaque tissue (*i.e.*, not detected in patient-matched buffy coats). Based on variant allele frequencies, we estimated that individual locally expanded clones contributed with up to 15% of plaque segment cell content. In addition, seven patients were CHIP carriers and in several of these patients, hematopoietic clones comprised over 30% of the cell population of plaque segments.

Taken together, we provide evidence that somatic mutations and clonal cell populations (expanded locally or invading from the circulation) are inherent features of atherosclerosis.

INTRODUCTION

Atherosclerosis is the focal accumulation of lipid, fibrous tissue, and cells in the intimal layer of arteries. The disease develops over decades and may suddenly manifest as myocardial infarction or ischemic stroke - leading causes of death in the world[1].

The cellular component of atherosclerotic plaques mainly originates from circulating myeloid cells and smooth muscle cells (SMCs) recruited from the local media[2]. Recent advances in the field have revised our perception of both sources: First, by use of multicolor lineage tracing in mouse models, it was unambiguously demonstrated that all SMC-derived plaque cells are progeny of few medial SMCs[3,4], thus reviving the hypothesis of monoclonality in atherosclerosis proposed by Benditt and Benditt almost 50 years ago[5].

Second, several lines of evidence now support an important role for clonal hematopoiesis of indeterminate potential (CHIP) in atherosclerotic cardiovascular disease[6-8]. Individuals with CHIP carry expanded hematopoietic clones often harboring mutations in epigenetic regulators (*e.g.*, *DNMT3A* and *TET2*)[9], which besides conferring a selective advantage render myeloid cells more inflammatory and pro-atherogenic[10].

Although these recent advances point to the involvement of clonal cell populations (either expanded locally in plaques or invading from the circulation) in the pathology of atherosclerosis, the extend of clonal populations partaking in human atherosclerosis remains elusive.

Recent studies have demonstrated that somatic mutations and clonal cell populations are present in a range of non-tumor tissues besides CHIP[11] (*e.g.*, skin[12], prostate[13], bladder[14], and esophagus[15]), and in various pathological conditions (*e.g.*, chronic liver disease[16], inflammatory bowel disease[17], and endometriosis[18]). There are indications that mutation-carrying clones partake in disease pathophysiology, and moreover, the burden of somatic mutations and clone sizes have been shown to aggravate with age and proposed to be involved in age-associated reduction of organ function[15,19].

In this study, we hypothesized that similar processes take place in human atherosclerotic plaques, and that interrogating the somatic mutational landscape of plaques may provide unprecedented insight into the potential involvement of clonal cell populations in atherosclerosis. Identification of mutations in single or few cells is challenging, but somatic mutations amplified by proliferative expansion of mutation-carrying cells can be detected by whole-exome sequencing of bulk tissue samples[18].

To address our hypothesis, we performed deep whole-exome sequencing of human atherosclerotic plaques and simultaneously sequenced buffy coat DNA from the same patients to evaluate whether detected mutations were confined to plaques (*i.e.*, not detected in buffy coats). In addition, parallel sequencing of plaque tissue and buffy coats

from the same individuals enabled us to investigate the contribution of circulating CHIP mutation-carrying cells in the plaque cell population.

RESULTS

Somatic mutations and clonal cell populations are inherent features of atherosclerosis

Whole-exome sequencing was performed on DNA extracted from carotid plaques and patient-matched buffy coats from 14 patients undergoing carotid endatherectomy (**supplementary table S1**). From each carotid plaque, one to four segments (2-5 mm tissue per segment) distanced 4-10 mm were analyzed in parallel (**fig. 1a**). The median sequencing depth across samples was 775X (IQR: 655-862) with an error rate of 3E-3 enabling accurate identification of mutations at variant allele frequencies (VAF) ≥ 1% with a variant read depth ≥ 5 (median: 18 (IQR: 13-26)) (**supplementary fig. S1**) (all sequencing metrics are shown in **supplementary table S2**).

We identified on average 26 (range: 2-83, median: 16.5, IQR: 11-40.25) somatic mutations per plaque (**fig. 1b**). These mutations were not detected in patient-matched buffy coats supporting local amplification of mutations by expansion of mutated cells (*i.e.*, clones).

VAFs ranged from 1% to 9.6% (median: 2.2%, IQR: 1.7-3%) (**supplementary fig. S2a**, **supplementary table S3**), representing clones constituting 1.3-15.4% (median: 4.3%, IQR: 3.3-5.9%) of plaque segment cell populations (**fig. 1c-d**, **supplementary fig. S2b**). Somatic mutations were detected in 29 of the 32 sequenced plaque segments (0-79 mutations per plaque segment, median: 6, IQR: 5.8-11.5), and six mutations were detected across several segments of a plaque requiring a physical extend of clones harboring these mutations of at least 4-16 mm (**fig. 1e**). To evaluate the number of cells constituting individual clones, we calculated the number of sequenced cells from plaque segment DNA yields, assuming 6 pg DNA per cell. Cell numbers ranged from 77,000 to 1,278,333 (median: 605,000, IQR: 418,333-820,833) resulting in cell number per clone estimates of 1,483-112,327 (median: 22,756, IQR: 12,432-37,285). Since DNA purifications may be sub-efficient, these are conservative lower-bound estimates.

Non-random distribution of somatic mutations

After establishing the existence of locally expanded clones, we sought to evaluate whether somatic mutations were clone *drivers*, *i.e.*, conferring a selective advantage (analogous to tumors), or merely amplified by coincidence as *passengers* in a clone expanding by other mechanisms.

We did not detect any mutational hotspots (as in CHIP[9] and certain types of cancer[20]), *i.e.,* genes mutated in several plaques. However, 17 of the mutated genes appeared in a recently reported compendium of 568 mutational cancer driver genes[20] (χ^2 test: $p < 0.001$).

To further investigate potential functional enrichment of mutated genes, we used two approaches. First, over-representation analysis of all 345 mutated genes showed enrichment of “metal ion transmembrane transporter”-,

"actin binding"-, "voltage-gated channel"-, and "protein tyrosine kinase"-activity terms (**fig. 1f**, **supplementary fig. S3a-b**). Tyrosine kinase activity typically mediates intracellular signaling associated with cell growth and motility implying potential clonal driver effects of these mutations, and mutated tyrosine kinases are frequently implicated in tumor development[21].

Second, as a complementary approach to assess functional enrichment, we used gene expression data from the gene-tissue expression (GTEx) portal[22] to compare distribution of gene expression levels of the 345 mutated genes with that of all genes of the genome (**fig. 1g**), and found the distribution to be skewed toward higher gene expression (χ^2 test: $p < 0.00001$). This was not specific for artery tissue as the same was observed in other tissues, such as liver and spleen (**supplementary fig. S4a-e**).

Taken together, although we did not identify hotspot clonal driver genes, our analyses indicated a non-random distribution of mutations throughout the exome. Although this implies that some somatic mutations contribute to clonal expansion, further experimentation is required to draw such conclusions.

Enrichment of mutational signatures

To gain more insight into mutational processes that could underlie the accumulation of somatic mutations in atherosclerotic plaques, we next investigated enrichment of mutational signatures. Across all patients, cytosine to thymine transitions (C>T) dominated the spectra, accounted for >40% of mutations (**supplementary fig. S5a**) and most frequently occurred next to a 3' guanine (**supplementary fig. S5b**) indicating methylation and de-amination as a possible mutational mechanism. Signature analysis revealed that the pattern of mutations largely resembled a combination of Catalogue of Somatic Mutations in Cancer (COSMIC)[23] mutational signatures previously associated with "thiopurine chemotherapy treatment" (SBS87), "tobacco smoking" (SBS5), "defective DNA mismatch repair" (SBS6) and "ultraviolet radiation" (SBS7a/b) (**supplementary fig. S5c-e**). Some of these terms are likely not relevant for a tissue that has not been exposed to chemotherapy or ultraviolet radiation, however, mutational signatures are annotated by association in the context of cancers, and future studies may unveil whether plaque-specific mutational processes result in similar signatures.

Circulating CHIP clones contribute to the plaque cell population

We next investigated the contribution of circulating CHIP mutation-carrying cells to the plaque cell population. By screening for mutations in 78 previously established CHIP genes[9] using buffy coat DNA, we found 7 of the 14 patients to be CHIP carriers, and several CHIP mutations were detected in each of these patients (**fig. 2a, supplementary table S4**). Buffy coat derived VAFs ranged from 1% to 17% (median: 5%, IQR: 2-6%) (**fig. 2a**)

corresponding to buffy coat clone cell frequencies of 2.1-34.7% (median: 9.7%, IQR: 4.3-11.2%). Except for a minor *DNMT3A* clone in patient 13, all CHIP clones were represented in patient-matched carotid plaques and were evenly distributed across plaque segments (**fig. 2b**). This distribution contrasted that of locally expanded clones, which was more confined to individual plaque segments. Indeed, this would be expected from a diffuse clonal population invading from the circulation as compared to more immobilized focally expanding clones within the plaque. CHIP clone fractions in buffy coats correlated with plaque fractions of the corresponding clones, and CHIP clones entering from the circulation in some patients contributed with more than 25% (median: 4.6%, IQR: 2.2-10.3%) of the cell population of individual plaque segments in several cases (**fig. 2c**).

DISCUSSION

In this study we used whole-exome sequencing to demonstrate that somatic mutations are inherent features of atherosclerotic plaques. Our findings suggest that the growth of atherosclerotic plaques does not result from simultaneous division of all cells at an equal rate. Rather, our findings are compatible with individual cells proliferating to form clones, which make up considerable portions of human carotid plaque cells. These observations add atherosclerosis to the growing number of non-cancerous diseases in which somatic mutations are present and potentially participate in disease development[24].

To identify somatic mutations at a high confidence level, we sequenced at high depth and used strict variant calling criteria. The reliability of reported mutations was supported by identification of matching mutations in independently sequenced plaque segments from the same patients and no reads supporting the mutations in the remaining samples, and as we identified matching CHIP mutations in patient-matched buffy coats and plaque segments. Additionally, the broad range of identified mutations across patients, and the occurrence of mutation-negative plaque segments indicate a negligible false-positive rate.

A limitation to the analytical approach employed in this study is the inability to assess distribution of mutations across clonal populations within each plaque. Few clones could harbor numerous mutations, and/or multiple clones could harbor few mutations (**supplementary fig. S6a-b**). Indeed, for six of the patients, the sum of clone cell frequencies estimated from each mutation exceeds 100%, excluding a scenario of a single mutation per clone in these patients. Moreover, our data do not allow us to pinpoint which cell type(s) clones are derived from or how clones are physically organized within plaque tissue.

Although our data indicate that the mutational spectrum is not random, it remains elusive to what extend somatic mutations contribute to clonal expansion. Indeed, as proposed for clonal expansion in mouse models[4,25], clone precursors may be a subset of cells possessing advantageous properties related to *e.g.*, proliferation, survival in a toxic plaque environment, or escaping counter-regulatory mechanisms of the immune system. Alternatively, a clone-founding cell could merely be located “at the right place at the right time” thereby be the first to supersede a stimulatory threshold for activation, and as previously proposed, the selected clone may simultaneously suppress expansion of neighboring cells through juxtacrine lateral inhibition[4]. In this scenario, randomly amplified passenger mutations detected by whole-exome sequencing would only represent a fraction of clones (**supplementary fig. S6c-d**). Finally, clonal patches carrying somatic mutations could already be present in the carotid artery prior to plaque development (**supplementary fig. S6e-f**).

In recent decades, the epidemiology of atherosclerotic cardiovascular disease has changed from being a disease of middle-aged smoking, hypercholesterolemic, hypertensive men, to increasingly being a disease of older people[26].

This epidemiological transition is attributed to the successes of lipid- and blood pressure-lowering medication and smoking cessation initiatives, as well as a growing ageing population in most countries[26]. As a consequence, the residual risk is increasingly attributed to age-related unknowns. The identification of CHIP as an age-associated independent risk factor highlights somatic mutations and clonally expanded cells as significant contributors to atherosclerotic cardiovascular disease[6,7]. The present study demonstrates that similar processes take place locally in plaque tissues, but to what extent local somatic mutations and clonal expansion contribute to disease development and residual risk remains to be investigated. Interestingly, a recent exploratory analysis of the CANTOS trial showed that CHIP carriers with *TET2* mutations displayed signicantly reduced relative risk (64%) of major cardiovascular events when treated with canakinumab (anti-IL1β antibody) as compared to non-CHIP carriers (reduced relative risk of 15%)[27]. This finding underscores the clinical relevance of understanding the biology of mutation-carrying clones in atherosclerotic cardiovascular disease. In the present study, we demonstrate that hematopoietic clones carrying mutations in *TET2* (and other CHIP genes) are not the only mutation-carrying clones that make up the plaque cell population. We envision that comprehending the biological underpinnings of clonal biology and phenotypic characteristics of expanding clones may unlock novel mechanisms to inhibit lesion development or increase plaque stability. To this end, another important notion from our study is that somatic mutations may serve as genetic tags for identification and characterization of clonal populations in future studies. This may prove to be a convenient tool for deciphering clonal biology in atherosclerosis to obtain unprecedented insight that could have implications for future therapeutics.

METHODS

Ethical approval and patient sample processing

The study was approved by the Danish National Committee on Health Research Ethics (Project ID: CVK-2006749) and The Regional Committees on Health Research Ethics for Southern Denmark (Project ID: S-20140202) and is registered in the Registry of Research Projects in the Region of Southern Denmark (file no. 18/20280).

Carotid plaque tissue and buffy coats from 14 later deceased patients who had undergone carotid endatherectomy either at the Department of Cardiac, Thoracic and Vascular Surgery, Odense University Hospital (OUH) or the Department of Vascular Surgery, Kolding Hospital were included in the study. Patients were admitted for surgery because of carotid plaque-associated symptoms. Informed consent was obtained from all participants prior to surgery.

Immediately after surgery, carotid plaque samples were placed and kept in ice cold Hanks Buffered Salt Solution containing 10 mM HEPES (Biological Industries, SKU BI-02-016-1A and BI-03-025-1B, respectively). Within 24 hours, plaques were sliced into 2 (patients 2, 4, 10, 13, and 14) or 5 mm thick segments (patients 1, 3, 5, 6, 7, 8, 9, 11, and 12) using a custom-made device. Every third segment was frozen at -80°C and stored in the Odense Artery Biobank infrastructure of the Centre for Individualized Medicine in Arterial diseases (CIMA) at OUH.

Blood was collected in EDTA vials, centrifuged at 4,000 x *g* for 10 minutes at 4°C, and buffy coats were collected using a pipette from the top of the centrifuged sample, and stored at -80°C in the Odense Artery Biobank.

Whole exome sequencing (WES) and data analysis

We performed whole exome sequencing on blood (buffy coat) and tissue samples obtained from 14 patients. Genomic DNA was isolated from fresh-frozen tissue samples and buffy coats using standard methods. The libraries were prepared using 50 ng DNA and Twist Comprehensive Exome Panel kit (Twist Bioscience, San Francisco, US), and 2x150bp pair-end sequencing was performed on an Illumina NovaSeq 6000 platform. Unique dual indexing was applied to reduce cross sample contamination from index hopping. Furthermore, unique molecular identifiers (UMI) from IDT were applied for error suppression.

Fastq files were aligned to reference sequence (human NCBI build 38) using the Burrows-Wheeler algorithm (BWA-MEM) version 0.7.12 and processed with the Genome Analysis Toolkit (GATK 4.2.0.0, gatk.broadinstitute.org) to generate recalibrated BAM files. Shortly, files were sorted using SortSam (version 1.3.1) and duplicates removed using MarkDuplicates (Picard Toolkit, version 2.25.0). Base quality score recalibration was done using BaseRecalibrator and ApplyBQSR to output post-recalibration BAM files used in the analysis. Raw data quality check

was done using FastQC (version 0.11.9). After data processing, Qualimap (version 2.2.2) and Picard were used to check mapping quality. Information gathered from Qualimap is shown regarding GC content, insert size, coverage, percentage of aligned bases, and general error rate. Information about mapping, and duplication rate was gathered using Picard.

Somatic mutations are called by finding mismatches present in a sample of interest and a matched normal sample. We sequenced both matched buffy coat and tissue samples at high coverage (767X on average, range 500X - 1141X of median coverage) to be able to identify with high confidence somatic variants and distinguish them from sequencing artifacts, even at lower variant allele frequencies (VAF). We set the lowest VAF at 1%, and discarded variants with under 5 reads.

To identify somatic variants occurring in the tissue samples and remove germline SNPs, Mutect2 joint variant-calling was performed on matched samples tissue vs. buffy coat. For very high sensitivity calling of variants identified in one sample, MuTect force calling was performed on all other samples. For the identification of single nucleotide variants and indels occurring in both buffy coat and frozen tissue, we used MuTect2 in single sample mode. Common single-nucleotide polymorphisms (SNPs) were removed by filtering against a panel of normal generated by the 1000 Genomes Project samples, and by using population allele frequencies of common and rare variants from the Genome Aggregation Database (gnomAD) (https://console.cloud.google.com/storage/browser/gatk-best-practices/). Variants were annotated using VarSeq version 2.2.1 (Golden Helix, Inc.) and filtered through a cascade of filters. Briefly, for variant calling in non-matched samples, the filters were: (i) variant is in a CHIP gene according to our list of 78 CHIP genes[9], (ii) the region is covered by at least 20 reads, (iii) has a known or predicted damaging effect on protein functionality (according to ClinVar or prediction tools), and (iv) has a minor allele frequency (MAF) < 1% (according to gnomAD). gnomAD is the world largest public collection of genetic variation, and it is based on 125,748 exomes and 15,708 whole-genomes collected worldwide (https://gnomad.broadinstitute.org/). We used the gnomAD collection from exome and genome sequencing data as a large external control group. For matched MuTect2 calling tissue vs. buffy coat, we selected variants with (i) at least 5 reads, (ii) a VAF in reads ≥ 1%, and no or very low signal in the buffy coat (< 0.01%), to eliminate variants that are present also in the buffy coat and were erroneously included by the variant calling process. Built-in post-calling filters in MuTect2 were used to select for high quality variants. A base quality threshold of 25 was set to accept a variant. All filtered variants were inspected manually using VarSeq; mapping artifacts and low-quality calls were removed.

For functional prediction of nonsynonymous variants we used the Combined Annotation Dependent Depletion (CADD Scores 1.4) method (PHRED scaled scores)[28]. The CADD algorithm includes conservation metrics, functional genomic data, exon-intron boundaries, and protein functionality scores. A score equal or greater of 20 indicates that a

variant is predicted to be among the 1% of the most deleterious substitutions. We used a CADD score of over 23 to select for a damaging effect. In addition, we used a dbNSFP tool (database for nonsynonymous single nucleotide polymorphisms' functional predictions) which incorporates five different algorithms (SIFT, Polyphen2, MutationTaster, MutationAssessor, and FATHMM)[29]. The most damaging variants were selected based on a voting system where four or all five of these algorithms predicted a negative functional impact.

Mutational signature analysis

Mutational signatures analysis was performed using the MutationalPatterns R packages (v3.6.0)[30]. Due to the limited number of mutations across all samples (n = 366), mutations were pooled to increase analytical power. A substitution catalogue was constructed from the frequency of the possible 96 trinucleotides. The low number of mutations did not enable us to extract any novel signatures. Instead, the catalogue of substitutions was fitted to the known COSMIC reference signatures (v3.2)[31].

To minimize the risk of overfitting and misattribution, the stricter refitting approach of MutationalPatterns was used. This approach starts with a standard fitting on all the COSMIC reference signatures and then in an iterative fashion removes the signature with the lowest contribution. In each iteration, the cosine similarity between the original and reconstructed profile is calculated. The iterations stop when the difference between two iterations becomes larger than a certain cutoff. To verify the stability of the resulting mutational signatures, the strict refitting was performed in 10,000 iterations using bootstrapping. We tested multiple cutoffs and found that a cutoff around 0.01 provided results that were stable through bootstrapping in the sense that they were included in the refitting solution 50% or more.

DISCLOSURES

The authors have nothing to declare.

DATA AVAILABILITY STATEMENT

The datasets generated and analyzed during the current study are not publicly available due to hospital guidelines and legislation regarding personal data. Data will be available from the corresponding author on reasonable request and with permission from Odensee University Hospital Legal Department.

ACKNOWLEDGEMENTS

We thank Mikkel Engstrøm Graversen for discussion of the statistical analyses used in the study.

FUNDING

The study was supported by a grant from Odense University Hospital to the Center for Individualized medicine in Arterial diseases (CIMA) and a grant from the Novo Nordisk Foundation to LMR (NNF20OC0065744).
LBS is supported by the Danish Diabetes Academy (supported by the Novo Nordisk Foundation).

REFERENCES

1 Diseases, G. B. D. & Injuries, C. Global burden of 369 diseases and injuries in 204 countries and territories, 1990-2019: a systematic analysis for the Global Burden of Disease Study 2019. *Lancet* **396**, 1204-1222, doi:10.1016/S0140-6736(20)30925-9 (2020).

2 Bjorkegren, J. L. M. & Lusis, A. J. Atherosclerosis: Recent developments. *Cell* **185**, 1630-1645, doi:10.1016/j.cell.2022.04.004 (2022).

3 Chappell, J. *et al.* Extensive Proliferation of a Subset of Differentiated, yet Plastic, Medial Vascular Smooth Muscle Cells Contributes to Neointimal Formation in Mouse Injury and Atherosclerosis Models. *Circ Res* **119**, 1313-1323, doi:10.1161/CIRCRESAHA.116.309799 (2016).

4 Jacobsen, K. *et al.* Diverse cellular architecture of atherosclerotic plaque derives from clonal expansion of a few medial SMCs. *JCI Insight* **2**, doi:10.1172/jci.insight.95890 (2017).

5 Benditt, E. P. & Benditt, J. M. Evidence for a monoclonal origin of human atherosclerotic plaques. *Proc Natl Acad Sci U S A* **70**, 1753-1756, doi:10.1073/pnas.70.6.1753 (1973).

6 Jaiswal, S. *et al.* Age-related clonal hematopoiesis associated with adverse outcomes. *N Engl J Med* **371**, 2488-2498, doi:10.1056/NEJMoa1408617 (2014).

7 Jaiswal, S. *et al.* Clonal Hematopoiesis and Risk of Atherosclerotic Cardiovascular Disease. *N Engl J Med* **377**, 111-121, doi:10.1056/NEJMoa1701719 (2017).

8 Libby, P. & Ebert, B. L. CHIP (Clonal Hematopoiesis of Indeterminate Potential): Potent and Newly Recognized Contributor to Cardiovascular Risk. *Circulation* **138**, 666-668, doi:10.1161/CIRCULATIONAHA.118.034392 (2018).

9 Marnell, C. S., Bick, A. & Natarajan, P. Clonal hematopoiesis of indeterminate potential (CHIP): Linking somatic mutations, hematopoiesis, chronic inflammation and cardiovascular disease. *J Mol Cell Cardiol* **161**, 98-105, doi:10.1016/j.yjmcc.2021.07.004 (2021).

10 Fuster, J. J. *et al.* Clonal hematopoiesis associated with TET2 deficiency accelerates atherosclerosis development in mice. *Science* **355**, 842-847, doi:10.1126/science.aag1381 (2017).

11 Lenormand, C. & Lipsker, D. Somatic Mutations in "Benign" Disease. *N Engl J Med* **385**, e34, doi:10.1056/NEJMc2110545 (2021).

12 Martincorena, I. *et al.* Tumor evolution. High burden and pervasive positive selection of somatic mutations in normal human skin. *Science* **348**, 880-886, doi:10.1126/science.aaa6806 (2015).

13 Grossmann, S. *et al.* Development, maturation, and maintenance of human prostate inferred from somatic mutations. *Cell Stem Cell* **28**, 1262-1274 e1265, doi:10.1016/j.stem.2021.02.005 (2021).

14 Lawson, A. R. J. *et al.* Extensive heterogeneity in somatic mutation and selection in the human bladder. *Science* **370**, 75-82, doi:10.1126/science.aba8347 (2020).

15 Martincorena, I. *et al.* Somatic mutant clones colonize the human esophagus with age. *Science* **362**, 911-917, doi:10.1126/science.aau3879 (2018).

16 Ng, S. W. K. *et al.* Convergent somatic mutations in metabolism genes in chronic liver disease. *Nature* **598**, 473-478, doi:10.1038/s41586-021-03974-6 (2021).

17 Olafsson, S. *et al.* Somatic Evolution in Non-neoplastic IBD-Affected Colon. *Cell* **182**, 672-684 e611, doi:10.1016/j.cell.2020.06.036 (2020).

18 Anglesio, M. S. *et al.* Cancer-Associated Mutations in Endometriosis without Cancer. *N Engl J Med* **376**, 1835-1848, doi:10.1056/NEJMoa1614814 (2017).

19 Cagan, A. *et al.* Somatic mutation rates scale with lifespan across mammals. *Nature* **604**, 517-524, doi:10.1038/s41586-022-04618-z (2022).

20 Martinez-Jimenez, F. *et al.* A compendium of mutational cancer driver genes. *Nat Rev Cancer* **20**, 555-572, doi:10.1038/s41568-020-0290-x (2020).

21 Saraon, P. *et al.* Receptor tyrosine kinases and cancer: oncogenic mechanisms and therapeutic approaches. *Oncogene* **40**, 4079-4093, doi:10.1038/s41388-021-01841-2 (2021).

22 Consortium, G. T. *et al.* Genetic effects on gene expression across human tissues. *Nature* **550**, 204-213, doi:10.1038/nature24277 (2017).

23 Tate, J. G. *et al.* COSMIC: the Catalogue Of Somatic Mutations In Cancer. *Nucleic Acids Res* **47**, D941-D947, doi:10.1093/nar/gky1015 (2019).

24 Mustjoki, S. & Young, N. S. Somatic Mutations in "Benign" Disease. *N Engl J Med* **384**, 2039-2052, doi:10.1056/NEJMra2101920 (2021).

25 Wang, Y. *et al.* Clonally expanding smooth muscle cells promote atherosclerosis by escaping efferocytosis and activating the complement cascade. *Proc Natl Acad Sci U S A* **117**, 15818-15826, doi:10.1073/pnas.2006348117 (2020).

26 Libby, P. The changing landscape of atherosclerosis. *Nature* **592**, 524-533, doi:10.1038/s41586-021-03392-8 (2021).

27 Svensson, E. C. *et al.* TET2-Driven Clonal Hematopoiesis and Response to Canakinumab: An Exploratory Analysis of the CANTOS Randomized Clinical Trial. *JAMA Cardiol* **7**, 521-528, doi:10.1001/jamacardio.2022.0386 (2022).

28 Rentzsch, P., Witten, D., Cooper, G. M., Shendure, J. & Kircher, M. CADD: predicting the deleteriousness of variants throughout the human genome. *Nucleic Acids Res* **47**, D886-D894, doi:10.1093/nar/gky1016 (2019).

29 Kircher, M. *et al.* A general framework for estimating the relative pathogenicity of human genetic variants. *Nat Genet* **46**, 310-315, doi:10.1038/ng.2892 (2014).

30 Manders, F. *et al.* MutationalPatterns: the one stop shop for the analysis of mutational processes. *BMC Genomics* **23**, 134, doi:10.1186/s12864-022-08357-3 (2022).

31 Alexandrov, L. B. *et al.* The repertoire of mutational signatures in human cancer. *Nature* **578**, 94-101, doi:10.1038/s41586-020-1943-3 (2020).

32 Wu, T. *et al.* clusterProfiler 4.0: A universal enrichment tool for interpreting omics data. *Innovation (N Y)* **2**, 100141, doi:10.1016/j.xinn.2021.100141 (2021).

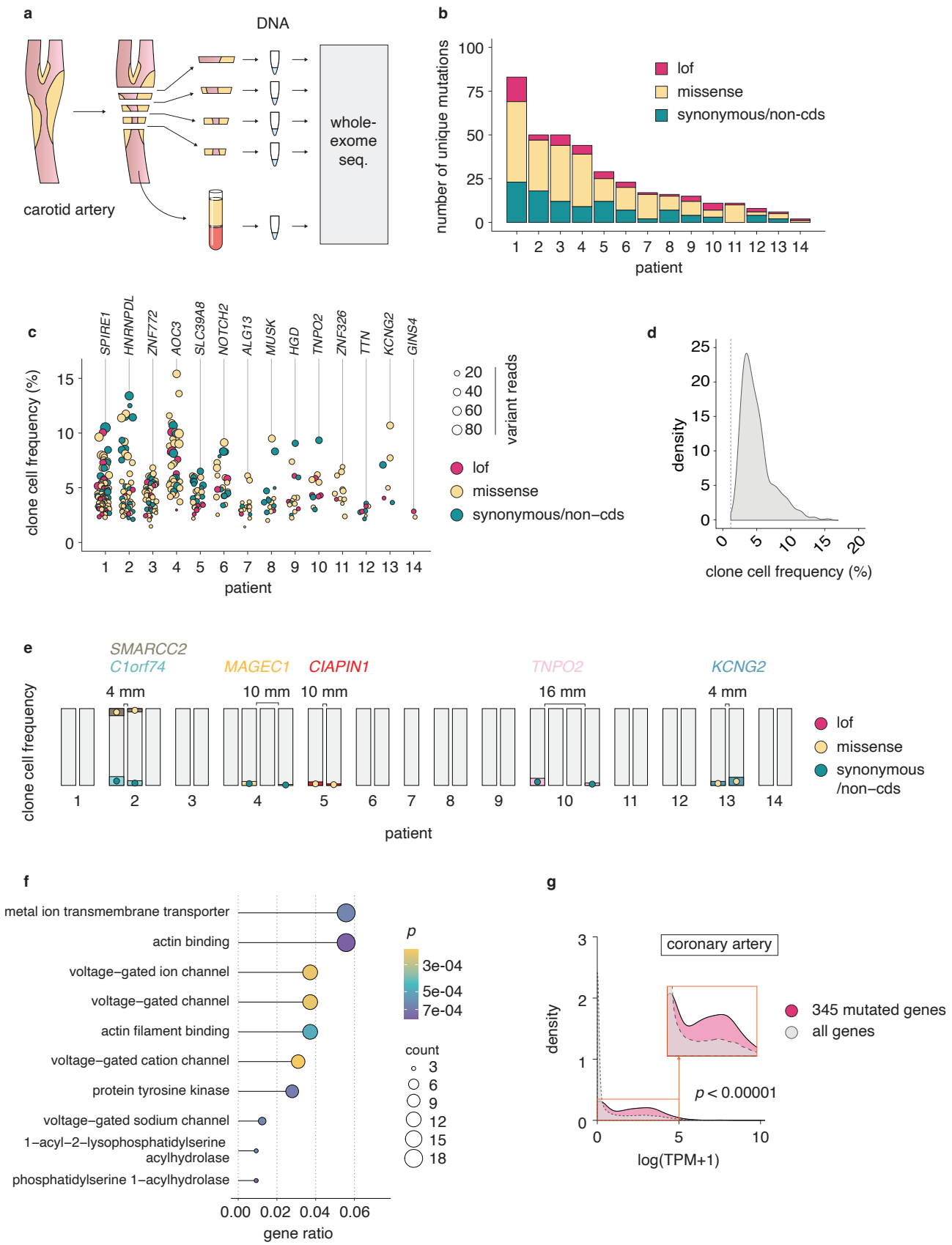
a
DNA
carotid artery
whole-exome seq.
b
number of unique mutations
100
75
50
25
0
lof
missense
synonymous/non-cds
1 2 3 4 5 6 7 8 9 10 11 12 13 14
patient
c
SPIRE1
HNRNPDL
ZNF772
AOC3
SLC39A8
NOTCH2
ALG13
MUSK
HGD
TNPO2
ZNF326
TTN
KCNG2
GINS4
clone cell frequency (%)
15
10
5
0
1 2 3 4 5 6 7 8 9 10 11 12 13 14
patient
20
40
60
80
variant reads
lof
missense
synonymous/non–cds
d
density
25
20
15
10
5
0
0 5 10 15 20
clone cell frequency (%)
e
SMARCC2
C1orf74
MAGEC1
CIAPIN1
TNPO2
KCNG2
4 mm
10 mm
10 mm
16 mm
4 mm
clone cell frequency
1 2 3 4 5 6 7 8 9 10 11 12 13 14
patient
lof
missense
synonymous /non–cds
f
metal ion transmembrane transporter
actin binding
voltage–gated ion channel
voltage–gated channel
actin filament binding
voltage–gated cation channel
protein tyrosine kinase
voltage–gated sodium channel
1–acyl–2–lysophosphatidylserine acylhydrolase
phosphatidylserine 1–acylhydrolase
0.00 0.02 0.04 0.06
gene ratio
p
3e-04
5e-04
7e-04
count
3
6
9
12
15
18
g
coronary artery
density
3
2
1
0
0 5 10
log(TPM+1)
p < 0.00001
345 mutated genes
all genes

Figure 1 | Locally expanded clone populations.
a. Carotid atherosclerotic plaques (one to four segments per plaque) and buffy coats from 14 patients undergoing carotid endatherectomy were analyzed by whole-exome sequencing. **b.** Barplot showing the number of plaque-confined somatic mutations (*i.e.*, mutations not identified in patient-matched buffy coats) for each patient. Mutation type is indicated by color. lof = loss of function; cds = coding sequence. **c.** Frequency of clone cells carrying a specific somatic mutation in carotid plaques. Clone cell frequencies are calculated based on the assumption of mutation heterozygosity by multiplying variant allele frequencies (VAFs) (shown in supplementary fig. S2a) by two, except for mutations located on the X-chromosome in male patients. Although single clones may harbor several mutations, each mutation is represented by separate clone cell frequencies on the plot. Mutation type is indicated by dot color, and variant reads is indicated by dot size. **d.** The density plot shows the distribution of clone cell frequencies calculated from each somatic mutation VAF from all patients (similar plots are shown for individual patients in supplementary fig. S2b). The dashed line shows the defined limit of detection. **e.** Six somatic mutations were detected in more than one plaque segment from the same patient. The total cell population within each plaque segment is represented by a grey bar, and the colored areas correspond to the fraction of cells harboring one of the six mutations. Mutation type is indicated by dot color. Intersegment distances used to estimate physical extends of clonal populations are indicated. **f.** Dotplot showing the ten most enriched molecular function gene ontology terms (using clusterProfiler 4.0 R package[32]) of the 345 genes mutated across all patients. Dot sizes indicate number of mutated genes for each term. The ratio shows the coverage of a given term by mutated genes, and dot colors indicate significance levels. **g.** Density plot showing the distribution of gene expression levels (presented as the logarithm of transcripts per million (TPM) +1) in coronary artery tissue (data from the gene-tissue expression (GTEx) portal[22], v8) for all genes of the genome and for the 345 mutated genes identified in carotid plaques. Area under the curves have been adjusted to be equal for the two datasets. To test if distributions were significantly different, a χ^2 test was performed based on the number of genes with expression levels above and below the median expression level of mutated genes, respectively.

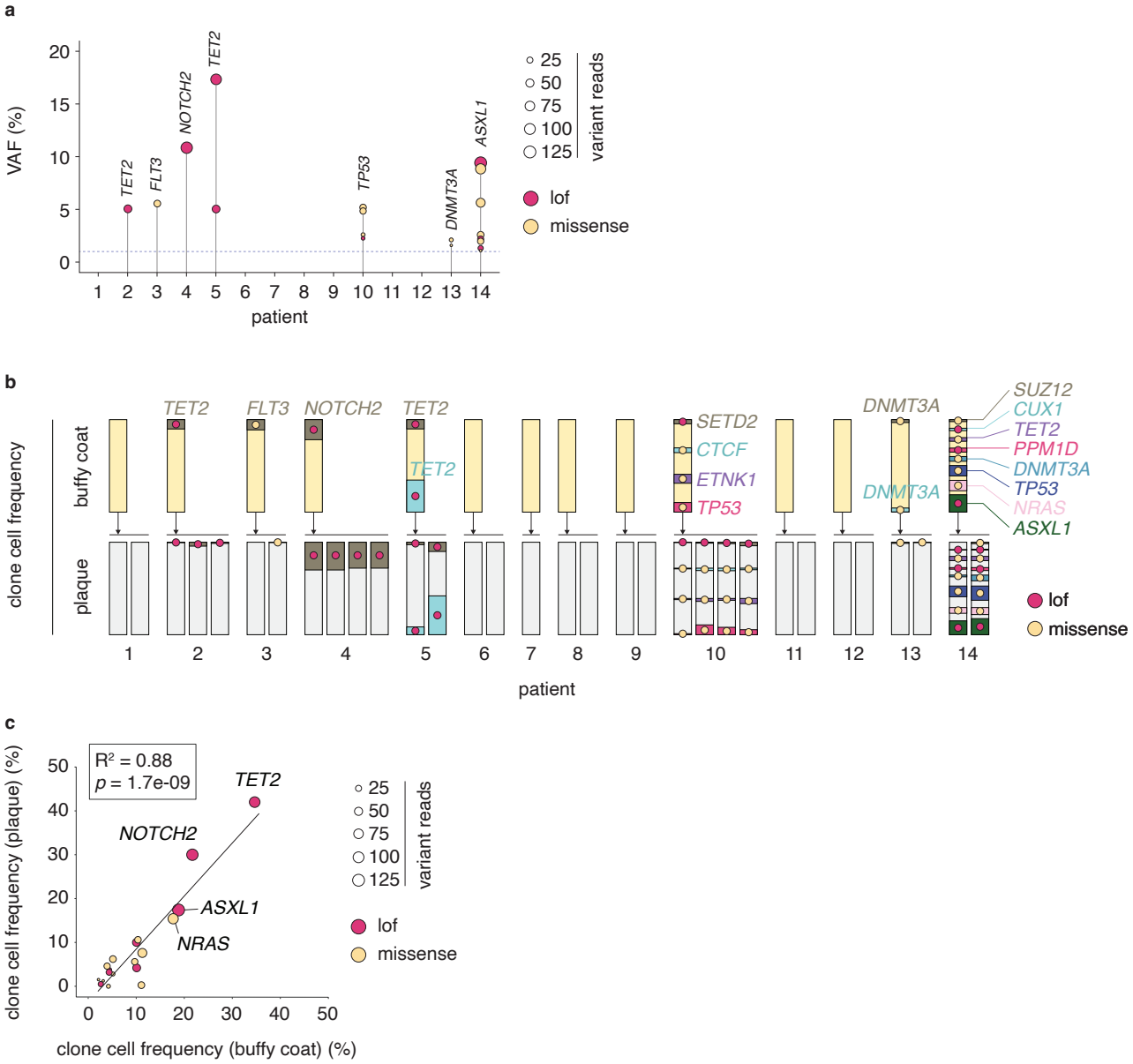

Figure 2 I Contribution of clonal hematopoiesis of indeterminate potential (CHIP) clones to the carotid plaque cell population.

a. Seven of the 14 patients were CHIP-carriers. The plot shows variant allele frequencies (VAFs) of CHIP mutations detected in buffy coats. For each patient, the identity of the mutated gene with the highest VAF is shown. Dot sizes indicate variant reads, and colors indicate the type of mutation. lof = loss of function. The dashed line shows the defined limit of detection. **b.** CHIP clone cell frequencies in buffy coats (yellow bars) and in plaque segments (grey bars) from the 14 patients. Clone cell frequencies are represented by colored areas within yellow and grey bars. Mutation type is indicated by dot color. **c.** Correlation of the frequency of CHIP cells carrying a particular somatic mutation in buffy coats and the maximal clone cell frequency across segments from patient-matched carotid plaques. CHIP gene identities are shown for the four clones with highest cell frequencies. Dot sizes indicate variant reads, and colors indicate the type of mutation. Statistics are based on *Pearson* correlation coefficient.

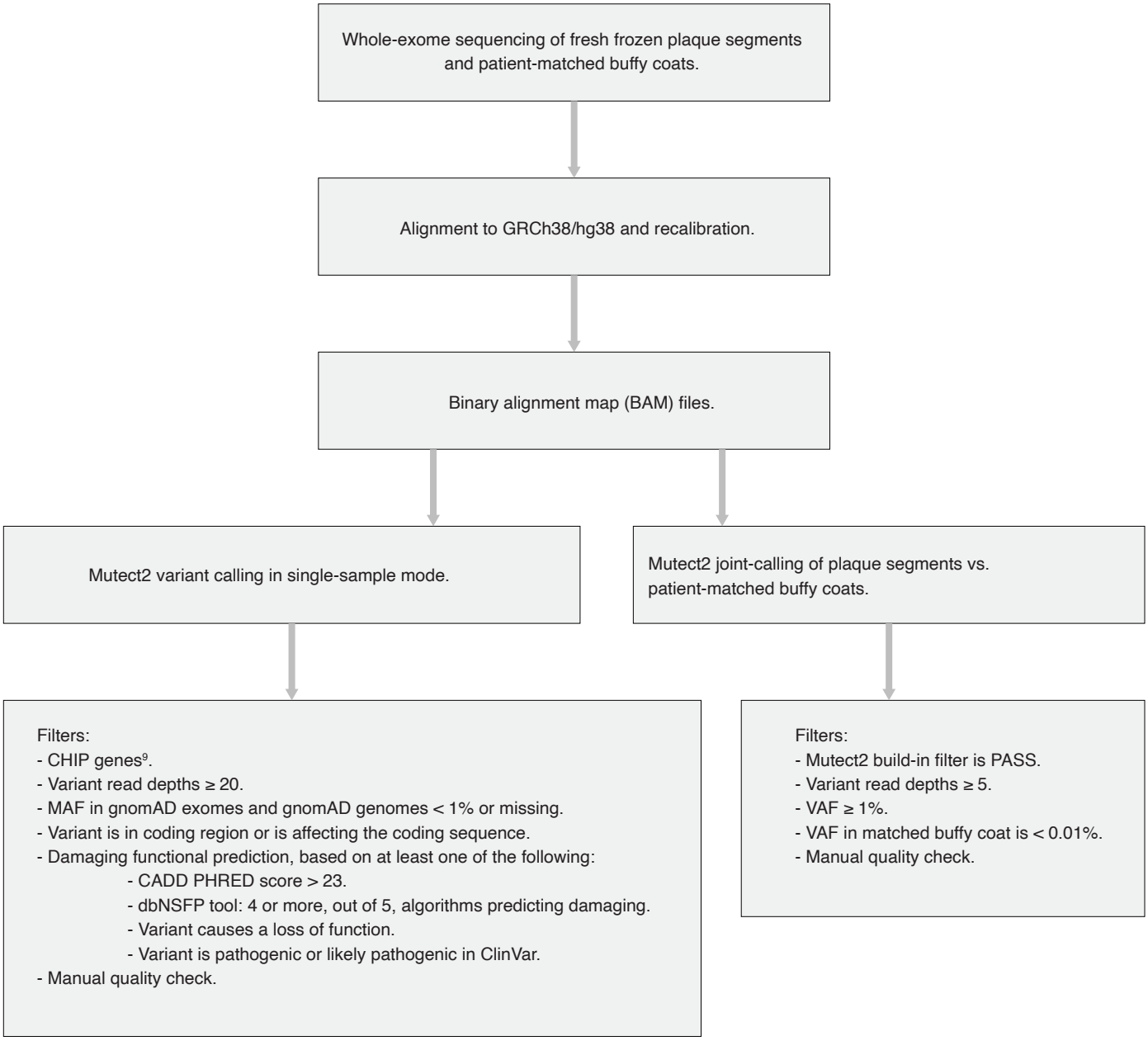

Supplementary figure S1 I
Flowchart showing the genetic analysis of the study. MAF (minor allele frequency); gnomAD (Genome Aggregation Database); CADD PHRED (Combined Annotation Dependent Depletion PHRED scale); VAF (variant allele frequency).

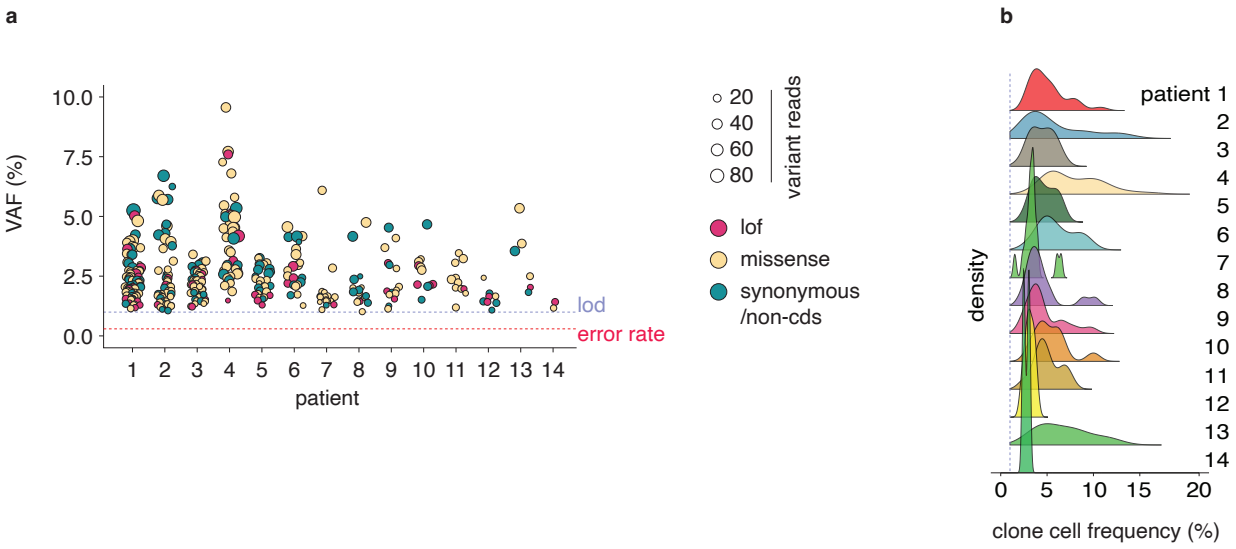

Supplementary figure S2 l

a. Variant allele frequencies (VAFs) of all plaque-confined somatic mutations (*i.e.*, mutations not identified in patient-matched buffy coats) for each patient. The horizontal dotted blue and red lines shows the defined limit of detection (lod) (1%) and sequencing error rate (0.3%), respectively. Dot sizes indicate variant reads, and colors indicate the type of mutation. lof = loss of function; cds = coding sequence. **b.** Density plot showing the distribution of clone cell frequencies calculated from each somatic mutation VAF from all individual patients.

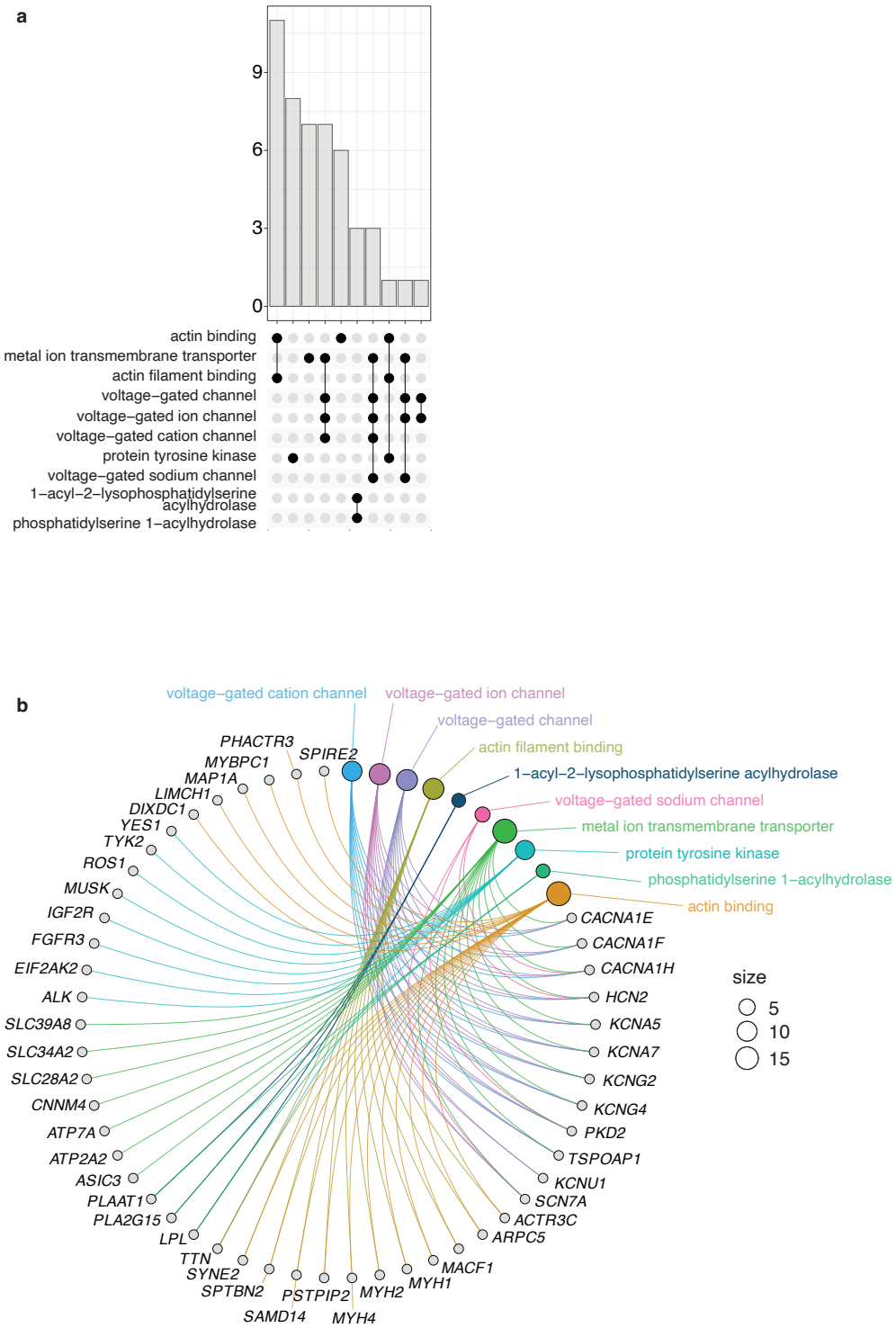

Supplementary figure S3 l

a. Upset plot showing overlaps among the top ten enriched molecular functions shown in fig. 1f. **b.** Circular network plot depicting the linkages of mutated genes with the top ten enriched molecular functions shown in fig. 1f. Sizes of dots representing molecular functions indicate the number of mutated genes attributed to each term.

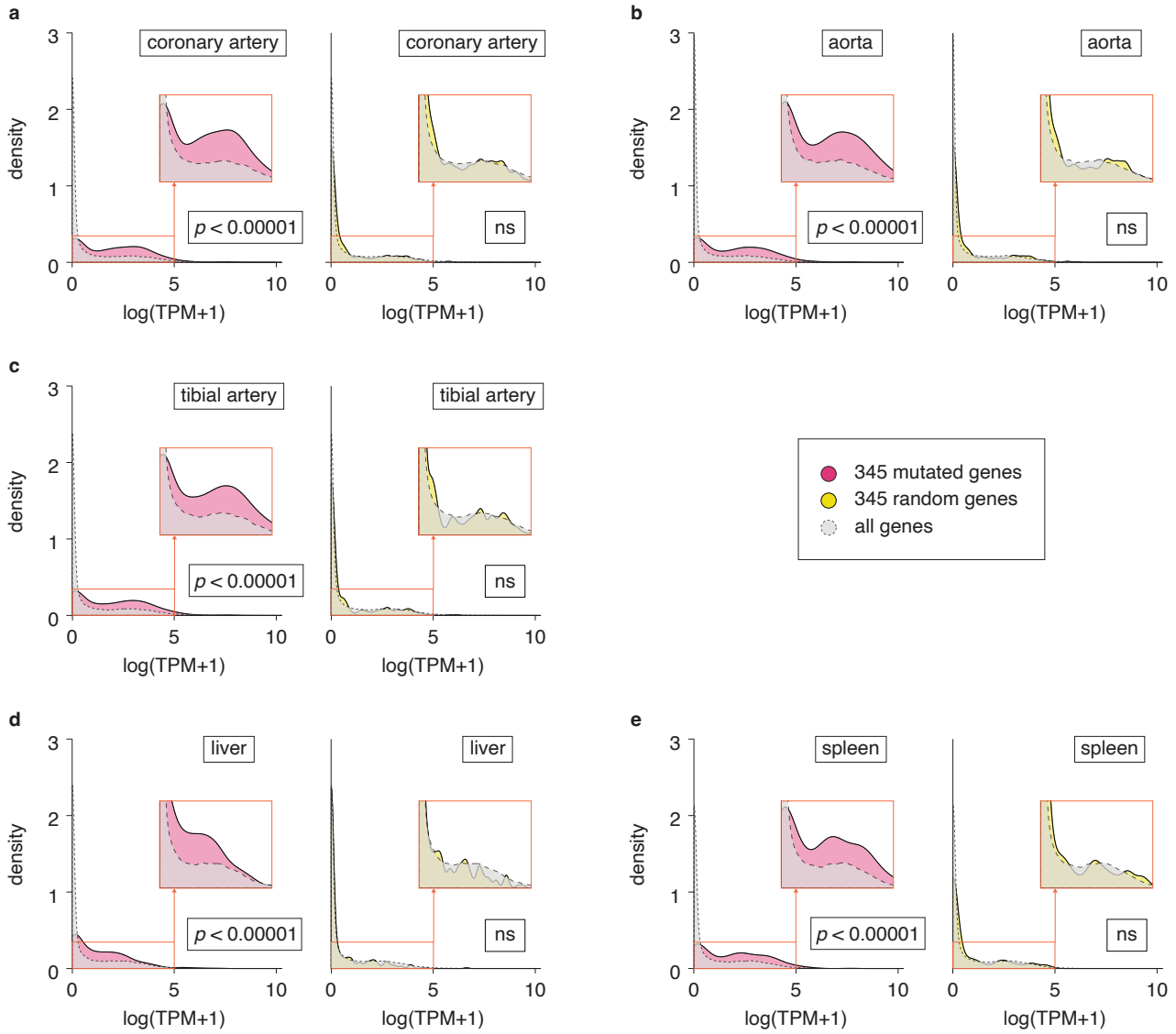

Supplementary figure S4 l

Density plot showing the distribution of gene expression levels (presented as the logarithm of transcripts per million (TPM) +1) in coronary artery- (**a**), aorta- (**b**), tibial artery- (**c**), liver- (**d**), and spleen- (**e**) tissue (data from the gene-tissue expression (GTEx) portal[22], v8) for 1) all genes of the genome, 2) the 345 mutated genes identified in carotid plaques, and 3) 345 genes randomly sampled from the genome. Area under the curves have been adjusted to be equal for the two datasets. To test if distributions within each graph were significantly different, a χ^2 test was performed based on the number of genes with expression levels above and below the median expression level of mutated genes or random genes, respectively.

The first graph of each panel shows that the 345 mutated genes identified in carotid plaques have significantly higher expression in all five tissue types as compared to all genes of the genome. The second graph in each panel shows that the expression level distribution of 345 randomly sampled genes would correspond to the distribution of all genes of the genome. The first panel in a is identical to fig. 1g but shown here to ease comparison with the other plots.

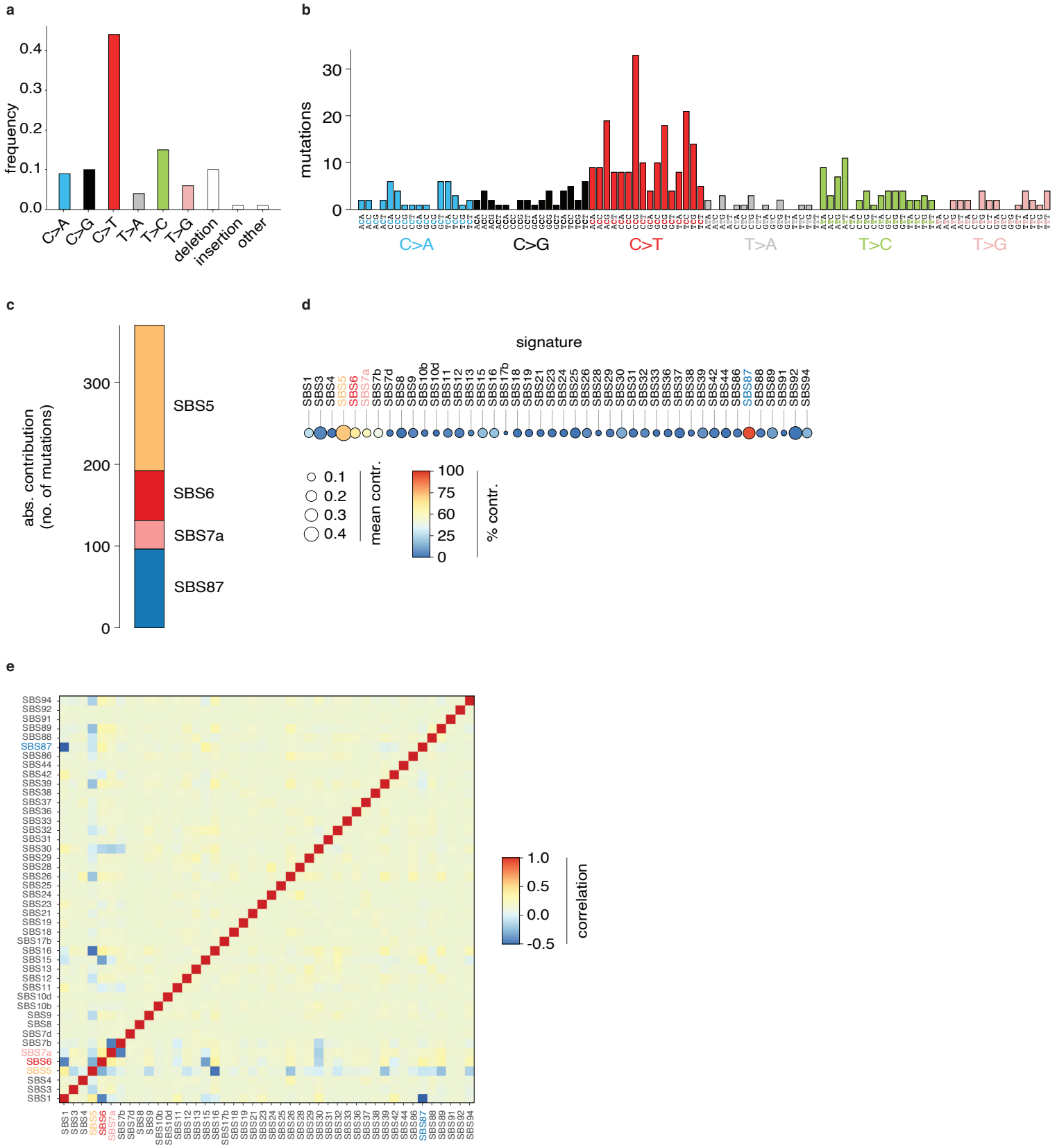

Supplementary figure S5 I

a. Frequency of mutations at the nucleotide level among all somatic mutations detected in carotid plaques. **b.** Catalogue of substitutions showing the frequency of trinucleotides *i.e.*, the substitution and the immediate flanking 3' and 5' nucleotides. **c.** Identified single base substitution (SBS) signatures using the strict refitting approach. **d.** Result of the bootstrapped fitting repeated 10,000 times. The identified signatures (c) all contributed to the bootstrapped solution 50% or more. **e.** Correlation between signatures. Negative correlation between signatures corresponds to their contribution being high in different bootstrap iterations. Several signatures compete for the same mutations in the refitting process due to similarities among signatures and limited number of mutations available.

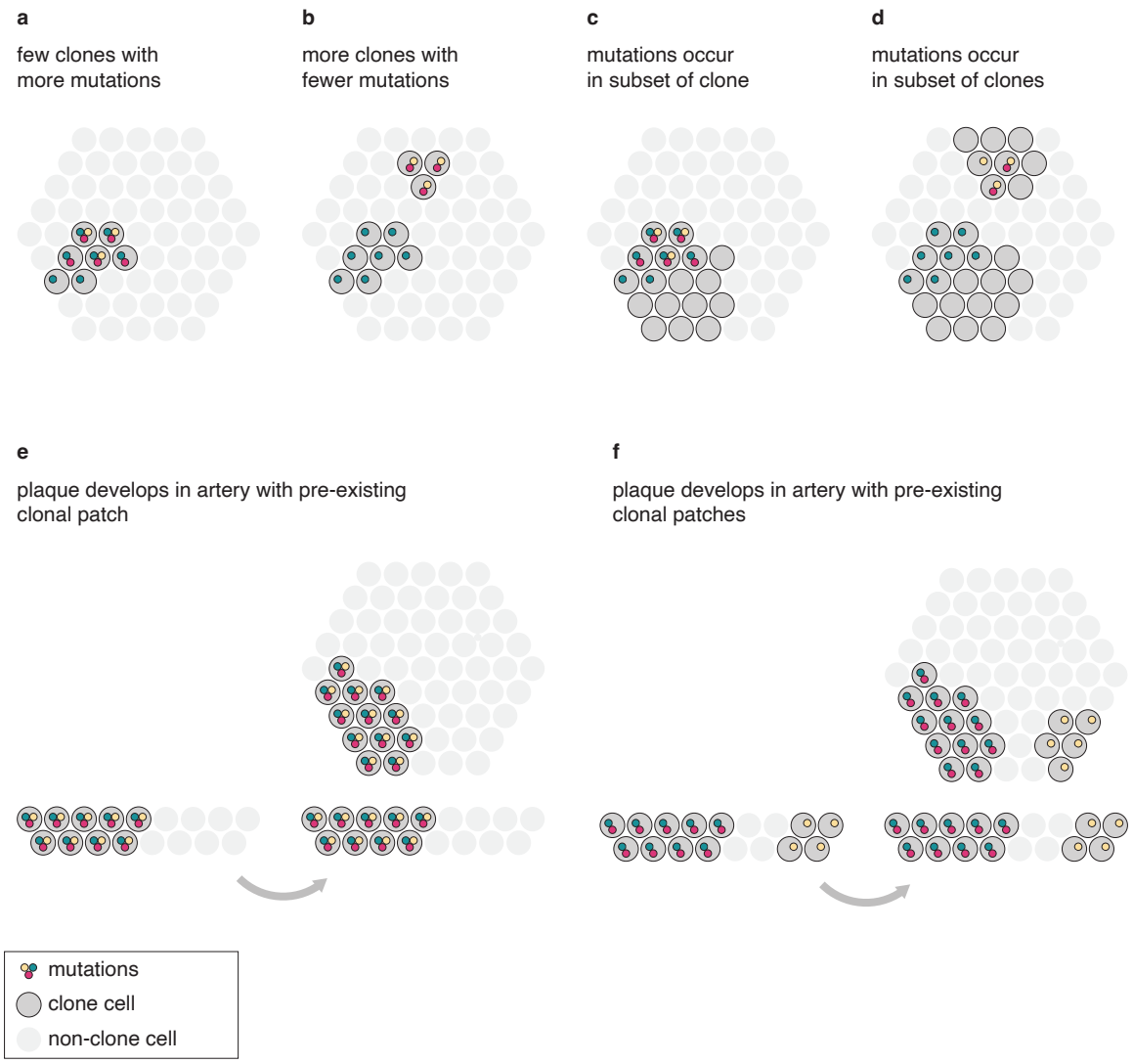

Supplementary figure S6 l
Possible scenarios underlying clonal cell frequencies deduced from somatic mutations.